Combustion Modeling and Kinetic Rate Calculations for a Stoichiometric Cyclohexane Flame. 1. Major Reaction Pathways†

Hongzhi R. Zhang,*,‡ Lam K. Huynh,§ Nawee Kungwan,§ Zhiwei Yang,‡ and Shaowen Zhang||

Department of Chemical Engineering, The University of Utah, Salt Lake City, Utah 84112, Department of Chemistry, The University of Utah, Salt Lake City, Utah 84112, and State Key Lab of Prevention and Control of Explosion Disasters, Beijing Institute of Technology, Beijing, China

Received: November 30, 2006; In Final Form: January 16, 2007

The Utah Surrogate Mechanism was extended in order to model a stoichiometric premixed cyclohexane flame ($P = 30$ Torr). Generic rates were assigned to reaction classes of hydrogen abstraction, β scission, and isomerization, and the resulting mechanism was found to be adequate in describing the combustion chemistry of cyclohexane. Satisfactory results were obtained in comparison with the experimental data of oxygen, major products and important intermediates, which include major soot precursors of C_2-C_5 unsaturated species. Measured concentrations of immediate products of fuel decomposition were also successfully reproduced. For example, the maximum concentrations of benzene and 1,3-butadiene, two major fuel decomposition products via competing pathways, were predicted within 10% of the measured values. Ring-opening reactions compete with those of cascading dehydrogenation for the decomposition of the conjugate cyclohexyl radical. The major ring-opening pathways produce 1-buten-4-yl radical, molecular ethylene, and 1,3-butadiene. The butadiene species is formed via β scission after a 1−4 internal hydrogen migration of 1-hexen-6-yl radical. Cascading dehydrogenation also makes an important contribution to the fuel decomposition and provides the exclusive formation pathway of benzene. Benzene formation routes via combination of C_2-C_4 hydrocarbon fragments were found to be insignificant under current flame conditions, inferred by the later concentration peak of fulvene, in comparison with benzene, because the analogous species series for benzene formation via dehydrogenation was found to be precursors with regard to parent species of fulvene.

Introduction

The Significance of Cyclohexane Chemistry. Liquid transportation fuels include significant fractions of naphthenes (cycloparaffins). Cyclohexane, for example, accounted for 8.6 vol % in the European Unleaded Certified Gasoline reported by Hakansson and co-workers.[1] Doute and co-workers[2] measured a fuel-rich premixed kerosene flame and reported that cycloparaffin fractions accounted for 10% of the fuel.

Cyclohexane and its derivatives are also preferred species in surrogate formulations. A surrogate fuel that included 10% methylcyclohexane[3] was used in our earlier study[4] to model the abovementioned premixed kerosene flame. Cathonnet and co-workers[5] assumed a surrogate fuel that was composed of cyclohexane, toluene, and *n*-decane in modeling a set of jet stirred reactor experiments with kerosene up to 40 atm. Mawid and co-workers[6] developed a detailed reaction model for JP-8 fuels using a 12-component surrogate, in which four naphthene species, methylcyclohexane, cyclooctane, tetralin, and decalin, were included. Cooke et al.[7] included a 20% fraction of methylcyclohexane in a surrogate for a JP-8 counter-flow diffusion flame.

The significant presence of naphthenes in commercial fuels is a major environmental concern because a much larger amount of benzene, a major soot precursor, was generated from flames of cyclohexanes, in comparison with other fuels.[8] This phenomenon is likely associated directly with the fuel structure, as concentrations of other aromatic precursors, such as acetylene, and C_3 and C_4 radicals, were comparable among flames with cyclohexane or other fuels. Also, cyclohexane produced significantly more benzene than those obtained from other fuels in a pulse flame combustor.[9] In an earlier modeling study,[4] we investigated the relative importance in benzene formation of each individual surrogate component in a premixed kerosene flame, and concluded that cyclohexanes in the fuel were major benzene sources.

Experimental, Kinetic and Modeling Studies of Cyclohexane. Most combustion experiments of naphthenes were operated on counter-flow diffusion flames and jet stirred reactor (JSR) flames. Voisin and co-workers,[10] for example, measured species concentrations in a JSR experiment of cyclohexane oxidation, at 10 atm and temperatures between 750 and 1100 K. Davis and Law[11] determined laminar flame speeds in atmospheric counter-flow twin flames for a wide range of equivalence ratios at room temperatures for C_1 to C_8 hydrocarbons that included cyclohexane and cyclopentane, and found that the flame speeds of cycloparaffins studied were close to those of the conjugate normal paraffins. Ristori and co-workers[12] reported concentration profiles for reactants, stable intermediates, and products in an atmospheric-pressure JSR experiment with *n*-propylcyclohexane at temperatures between 950 and 1250 K with a range of equivalence ratios between 0.5 and 1.5. Cooke and co-workers[7] measured the temperature profile and rich extinction limits in a JP-8 counter-flow diffusion flame, and Hakansson and co-workers[1] reported the chemical structure of

† Part of the special issue "James A. Miller Festschrift".

* Corresponding author. Phone: (801) 349-8680. Fax: (801) 585-5607. E-mail: westshanghai@yahoo.com.

‡ Department of Chemical Engineering, The University of Utah.

§ Department of Chemistry, The University of Utah.

|| Beijing Institute of Technology.

10.1021/jp068237q CCC: $37.00
Published on Web 02/23/2007

a stoichiometric atmospheric premixed flame with the European Unleaded Certified Gasoline. In both studies, cyclohexane or other naphthenes were included to be major fractions for the composite fuels of JP-8 and gasoline.

A few studies on reaction kinetics of cyclohexane and its derivatives complement combustion experiments with naphthenes. Braun-Unkhoff et al.,[13] for example, investigated the initial product channels of cyclohexane pyrolysis when very thin fractions of the fuel in the unburned mixture were heated behind reflected shock waves up to 1900 K at 1.5−2 atm. Bennett and co-workers[14] published an interesting study on decomposition pathways of isotopically labeled cyclohexanes in a single-cylinder engine, by monitoring the isotopic distributions of cyclohexane, cyclohexene, benzene, 1,3-butadiene, and propylene in the exhausted gas. Ranzi et al.[15] have published an excellent review of the use of lumping techniques for detailed kinetic modeling of hydrocarbon mixtures that were extended to include naphthenes. A mechanism generation technique using generic rates for reactions that involve paraffins, alkyl radicals, and olefins was proposed in our earlier publication,[16] and the resulting Utah Surrogate Mechanism was validated with measured concentration profiles and flame speeds in 40 premixed flames with fuels from C_1 to C_{16} that include cyclohexane and composite fuels of gasoline and kerosene.

In addition to kinetic studies, a few reaction models have been published in order to simulate combustion of naphthenes for various experiments. Klai and Baronnet[17] proposed a cyclohexane oxidation mechanism that included approximately 30 reactions, and the mechanism was used to simulate the observed product distribution in a static reaction vessel operated by the same authors. A previously validated C_1-C_5 mechanism was extended by Voisin and co-workers,[10] and was used to model measured concentrations in a JSR experiment with cyclohexane. This mechanism was extended, later on, in order to predict concentration profiles in cyclohexane flames under the same experimental conditions except at lower pressures with a range of equivalence ratios between 0.5 and 1.5.[18] Satisfactory results were obtained for most species. The mechanism was also validated with flame speed data measured in counter-flow twin flames.

Ristori and co-workers[12] compiled a reaction mechanism of *n*-propylcyclohexane that included 176 species and 1369 reactions, and the mechanism was used to study the oxidation of *n*-propylcyclohexane in a JSR. Granata and co-workers[19] presented a mechanism that described the pyrolysis and combustion of cyclohexane and methylcyclohexane using a lumping technique. Isomerization via intramolecular hydrogen transfer, which competes with β scission, was critically examined. The mechanism included both low- and high-temperature chemistry, and was validated with ignition delay times obtained in a rapid compression machine and closed vessels, and also with concentration profiles measured in jet stirred reactors and a turbulent plug flow reactor.

The Granata mechanism was only a subset of the larger Ranzi mechanism[15] that was used to model the temperature profile and rich extinction limits in a JP-8 counter-flow diffusion flame[7] and the concentration profiles of selected species in a kerosene premixed flame.[3] Mawid et al.[6] proposed another reaction mechanism of JP-8 that included four naphthene components, and the mechanism predicted ignition data better for higher initial temperatures.

The major competing formation pathways of benzene and 1,3-butadiene, two main fuel decomposition products, will be proposed in this work, and predicted concentrations will be compared with experimental measurements. The proposed mechanism will elaborate the significance of isomerization between fuel conjugate species in the product distribution. Also proposed are the interweaving dehydrogenation pathways between the benzene and toluene homologous series as vital mechanisms for the formation of single-ring aromatic species including benzene, complementing our earlier results of cascading dehydrogenation routes for the benzene formation from cyclohexane and methylcyclohexane.[4,16] The precursor relationship between critical species is also one of the foci of this study, in order to reveal the uniqueness of the cyclohexane decomposition mechanism.

Reaction Mechanism and Experimental Data

In the combustion mechanism of methylcyclohexane (MCH) in the Utah Surrogate Mechanism that was developed to simulate combustion of liquid transportation fuels,[4,16] fuel consumption pathways were assigned generic rates and a lumping technique was used with the assumption that hydrogen abstraction is the controlling step. Benzene formation via dehydrogenation of the substituted ring was critically examined, and good agreement was obtained between the experimental and predicted benzene concentrations in kerosene and gasoline flames.

It will be very valuable if our proposed mechanism can be validated directly with flame data of cyclohexane or its derivatives that cover a temperature range from 500 to 800 K at the burner surface to approximately 1800 to 2200 K at the post flame zone. Experimental studies of premixed cyclohexane flames were not available until recently when the structures of premixed cyclohexane flames were measured by Westmoreland and co-workers at two equivalence ratios of 1.0[8] and 2.0,[20] using photoionization molecular beam mass spectrometry (MBMS). When this work was reviewed, Westmoreland and co-workers published a parallel study reporting experimental data of the stoichiometric cyclohexane flame,[21] as well as modeled results of selected species, i.e., cyclohexene, 1,3-cyclohexadiene, and benzene. Both the current and parallel studies propose generally similar ideas of benzene formation via dehydrogenation, which is consistent with our earlier studies[4,16] of mechanisms of cyclohexane and its derivatives that were used in kerosene and gasoline flame modeling. Divergences of kinetic details between the current and parallel studies will be discussed in this work. Notable differences include the role of conjugate alkyl radical isomerization, and the formation of fulvene and butadiene, among others.

In this study, the Utah Surrogate Mechanism was refined in order to reproduce the details of the stoichiometric premixed cyclohexane flame (fuel:O_2:Ar = 6.75:60.75:32.5%) at 30 Torr measured by Law.[8,21] The simulator used was CHEMKIN IV,[22] and thermodynamics data for the gaseous species were obtained from the CHEMKIN thermodynamic database[23] or estimated by THERGAS[24] employing Benson's additivity theory.[25] Transport properties of species were obtained from the CHEMKIN transport database[26] or estimated from those of similar species.

Mechanism Generation Methodology

Fuel Consumption Reactions. Selected reactions in the extended Utah Surrogate Mechanism that are relevant to the cyclohexane dcomposition are listed in Table 1. Generic rates have been used extensively in the extended mechanism, and these rates were reported elsewhere.[16] Thermodynamic data of selected species that are most relevant to this work are compared in Table 2 with literature values from NIST Chemistry WebBook[27,28] and Burcat and Ruscic.[29]

TABLE 1: Selected Reactions in the Cyclohexane Decomposition Submechanism

		$k = AT^n \exp(-E/RT)$, mol·cm·s·cal			
no.	reaction	*A*	*n*	*E*	reference
		Fuel Decomposition			
R1	c-C_6H_{12} + H = c-C_6H_{11} + H_2	7.80×10^6	2.4	4 471.08	generic[a]
R2	c-C_6H_{12} + OH = c-C_6H_{11} + H_2O	2.82×10^8	1.61	−34.89	generic
R3	c-C_6H_{12} + O = c-C_6H_{11} + OH	1.86×10^6	2.5	2 230	generic
R4	c-C_6H_{12} + CH_3 = c-C_6H_{11} + CH_4	1.62×10^5	2.26	7 287.05	generic
R5	c-C_6H_{12} + HO_2 = c-C_6H_{11} + H_2O_2	1.34×10^{14}	0	17 690	generic
R6	c-C_6H_{12} + O_2 = c-C_6H_{11} + HO_2	1.20×10^{14}	0	50 150.1	generic
R7	c-C_6H_{12} = 1-C_6H_{12}	5.01×10^{16}	0	88 230	Tsang[33]
R8	c-C_6H_{11} = 1-C_6H_{11}-6	1.60×10^{13}	0	28 300	generic
R9	1-C_6H_{11}-6 = 1-C_6H_{11}-3	2.00×10^{11}	0	14 100	generic − 1 kcal
R10	1-C_6H_{11}-6 = 1-C_6H_{11}-2	1.00×10^{11}	0	16 100	generic + 2 kcal
R11	1-C_6H_{11}-6 = 1-C_6H_{11}-1	1.00×10^{11}	0	20 100	generic + 2 kcal
R12	1-C_6H_{11}-6 = BC_4H_7 + C_2H_4	3.20×10^{13}	0	28 400	generic
R13	1-C_6H_{11}-3 = C_2H_5 + $CH_2CHCHCH_2$	1.60×10^{13}	0	28 300	generic
R14	1-C_6H_{11}-3 = CH_3 + L-C_5H_8	2.38×10^8	0.88	29 600	Matheu et al.[35]
R15	1-C_6H_{11}-1 = C_2H_2 + PC_4H_9	1.60×10^{13}	0	28 300	generic
R16	1-C_6H_{11}-2 = AC_3H_4 + NC_3H_7	1.60×10^{13}	0	28 300	generic
		Cascading Dehydrogenation, Benzene			
R17	c-C_6H_{11} = c-C_6H_{10} + H	1.00×10^{14}	0	38 000	Dean[37,b]
R18	c-C_6H_{11} + O_2 = c-C_6H_{10} + HO_2	4.00×10^{12}	0	4 251.19	generic
R19	c-C_6H_{11} + O = c-C_6H_{10} + OH	1.81×10^{14}	0	0	Tsang[38]
R20	c-C_6H_{11} + OH = c-C_6H_{10} + H_2O	4.84×10^{13}	0	0	Tsang[38]
R21	c-C_6H_{11} + H = c-C_6H_{10} + H_2	3.60×10^{12}	0	0	Tsang[38]
R22	c-C_6H_{11} + CH_3 = c-C_6H_{10} + CH_4	6.04×10^{12}	−0.32	0	Tsang[38]
R23	c-C_6H_{10} = c-C_6H_9-3 + H	5.01×10^{15}	0	81 700	Dean[37]
R24	c-C_6H_{10} + H = c-C_6H_9-3 + H_2	2.60×10^6	2.4	4 471.08	generic
R25	c-C_6H_{10} + OH = c-C_6H_9-3 + H_2O	9.40×10^7	1.61	−34.89	generic
R26	c-C_6H_{10} + O = c-C_6H_9-3 + OH	6.20×10^5	2.5	2 230	generic
R27	c-C_6H_{10} + CH_3 = c-C_6H_9-3 + CH_4	5.40×10^4	2.26	7 287.05	generic
R28	c-C_6H_{10} + HO_2 = c-C_6H_9-3 + H_2O_2	4.47×10^{13}	0	17 690	generic
R29	c-C_6H_{10} + O_2 = c-C_6H_9-3 + HO_2	4.00×10^{13}	0	50 150.1	generic
R30	c-C_6H_{10} + M = c-C_6H_9-4 + H + M	1.00×10^{16}	0	95 000	Dean[37]
R31	c-C_6H_{10} + H = c-C_6H_9-4 + H_2	2.60×10^6	2.4	4 471.08	generic
R32	c-C_6H_{10} + OH = c-C_6H_9-4 + H_2O	9.40×10^7	1.61	−34.89	generic
R33	c-C_6H_{10} + O = c-C_6H_9-4 + OH	6.20×10^5	2.5	2 230	generic
R34	c-C_6H_{10} + CH_3 = c-C_6H_9-4 + CH_4	5.40×10^4	2.26	7 287.05	generic
R35	c-C_6H_{10} + HO_2 = c-C_6H_9-4 + H_2O_2	4.47×10^{13}	0	17 690	generic
R36	c-C_6H_{10} + O_2 = c-C_6H_9-4 + HO_2	4.00×10^{13}	0	50 150.1	generic
R37	c-C_6H_9-3 + O_2 = c-C_6H_8 + HO_2	2.00×10^{12}	0	4 251.19	generic
R38	c-C_6H_9-3 + H = c-C_6H_8 + H_2	1.80×10^{12}	0	0	Tsang[38]
R39	c-C_6H_9-3 + OH = c-C_6H_8 + H_2O	2.42×10^{13}	0	0	Tsang[38]
R40	c-C_6H_9-3 ⇒ c-C_6H_8 + H	3.16×10^{12}	0	36 960	Weissman et al.[39,c]
R41	c-C_6H_9-4 + O_2 = c-C_6H_8 + HO_2	2.00×10^{12}	0	4 251.19	generic
R42	c-C_6H_9-4 + H = c-C_6H_8 + H_2	1.80×10^{12}	0	0	Tsang[38]
R43	c-C_6H_9-4 + OH = c-C_6H_8 + H_2O	2.42×10^{13}	0	0	Tsang[38]
R44	c-C_6H_9-4 = c-C_6H_8 + H	3.16×10^{12}	0	36 960	Weissman et al.[39]
R45	c-C_6H_9-4 = C_2H_3 + $CH_2CHCHCH_2$	1.00×10^{13}	0	38 000	generic, +10 kcal/mol[d]
R46	c-C_6H_8 + H = c-C_6H_7 + H_2	7.80×10^6	2.4	3 000	generic × 3 − 1.5 kcal
R47	c-C_6H_8 + OH = c-C_6H_7 + H_2O	2.82×10^8	1.61	−1 500	generic × 3 − 1.5 kcal
R48	c-C_6H_8 + O = c-C_6H_7 + OH	1.86×10^6	2.5	2 230	generic × 3
R49	c-C_6H_8 + CH_3 = c-C_6H_7 + CH_4	1.62×10^5	2.26	7 287.05	generic × 3
R50	c-C_6H_8 + O_2 = c-C_6H_7 + HO_2	1.20×10^{14}	0	50 150.1	generic × 3
R51	c-C_6H_8 + HO_2 = c-C_6H_7 + H_2O_2	1.34×10^{14}	0	17 690	generic × 3
R52	c-C_6H_8 = c-C_6H_7 + H	5.00×10^{13}	0	72 530	Dean[37]/100
R53	c-C_6H_7 = bC_6H_6 + H	7.90×10^{11}	0	28 420	Dean[37]/40
R54	c-C_6H_7 + O_2 = bC_6H_6 + HO_2	2.00×10^{12}	0	4 251.19	generic
R55	c-C_6H_7 + H = bC_6H_6 + H_2	1.80×10^{12}	0	0	Tsang[38]
R56	c-C_6H_7 + OH = bC_6H_6 + H_2O	2.42×10^{13}	0	0	Tsang[38]
R57	c-C_6H_7 = CH_3-c-C_5H_4	5.00×10^{12}	0	38 100	Ritter et al.[44]
R58	bC_6H_6 + H = CH_3-c-C_5H_4	2.39×10^{27}	−3.92	29 200	Ritter et al.[44]
R59	CH_3-c-C_5H_4 = fC_6H_6 + H	1.00×10^{14}	0	38 000	Doute et al.[53,e]
R60	CH_3-c-C_5H_4 + O_2 = fC_6H_6 + HO_2	2.00×10^{12}	0	4 251.19	generic
R61	CH_3-c-C_5H_4 + H = fC_6H_6 + H_2	1.80×10^{12}	0	0	Tsang[38,f]
R62	CH_3-c-C_5H_4 + OH = fC_6H_6 + H_2O	2.42×10^{13}	0	0	Tsang[38,f]
R63	CH_3-c-C_5H_4 + H = CH_3-c-C_5H_5	1.00×10^{14}	0	0	Marinov et al.[49]
R64	CH_3-c-C_5H_4 + H = CH_3 + C_5H_5	1.00×10^{14}	0	0	Marinov et al.[49]
R65	CH_3-c-C_5H_5 = fC_6H_6 + H_2	2.51×10^{14}	0	59 020	Alfassi et al.[54,g]
R66	fC_6H_6 + H = bC_6H_6 + H	3.00×10^{12}	0.5	2 000	Marinov et al.[49]
R67	H_2CCCH + AC_3H_5 = fC_6H_6 + H + H	1.00×10^{12}	0	3 000	Burcat et al.[55]/2

TABLE 1 (Continued)

no.	reaction	$k = AT^n \exp(-E/RT)$, mol·cm·s·cal A	n	E	reference
	Cascading Dehydrogenation, Toluene				
R68	$C_6H_{11}CH_3 = c\text{-}C_6H_{11} + CH_3$	1.26×10^{16}	0	88 030	Brown and King[47]
R69	$C_6H_9CH_3 + M = c\text{-}C_6H_9\text{-}3 + CH_3 + M$	7.94×10^{16}	0	68 560	Trenwith[56,h]
R70	$C_6H_9CH_3 + M = c\text{-}C_6H_9\text{-}4 + CH_3 + M$	7.94×10^{16}	0	68 560	Trenwith[56,h]
R71	$C_6H_7CH_3 + M = c\text{-}C_6H_7 + CH_3 + M$	8.32×10^{15}	0	66 370	Trenwith[57,i]
R72	$C_6H_9CH_3 + H = C_6H_7CH_3 + H + H_2$	5.00×10^{6}	2.4	4 000	Zhang et al.[16]
R73	$C_6H_9CH_3 + OH = C_6H_7CH_3 + H + H_2O$	1.88×10^{8}	1.6	−40.70	Zhang et al.[16]
R74	$C_6H_9CH_3 + H = c\text{-}C_6H_8 + CH_3 + H_2$	5.00×10^{6}	2.4	3 500	Zhang et al.[16]
R75	$C_6H_9CH_3 + OH = c\text{-}C_6H_8 + CH_3 + H_2O$	1.88×10^{8}	1.6	−40.7	Zhang et al.[16]
R76	$C_6H_9CH_3 + H = c\text{-}C_6H_{10} + CH_3$	2.27×10^{13}	0	3 569.38	generic
R77	$C_6H_7CH_3 + H = C_6H_5CH_3 + H + H_2$	2.50×10^{6}	2.4	3 500	Zhang et al.[16]
R78	$C_6H_7CH_3 + OH = C_6H_5CH_3 + H + H_2O$	9.38×10^{7}	1.61	−34.89	Zhang et al.[16]
R79	$C_6H_7CH_3 + H = bC_6H_6 + CH_3 + H_2$	1.30×10^{6}	2.4	3 500	Zhang et al.[16]
R80	$C_6H_7CH_3 + OH = bC_6H_6 + CH_3 + H_2O$	4.69×10^{7}	1.6	−40.7	Zhang et al.[16]
R81	$C_6H_7CH_3 + H = c\text{-}C_6H_8 + CH_3$	2.27×10^{13}	0	3 569.38	generic
R82	$C_6H_5CH_3 + H = bC_6H_6 + CH_3$	1.20×10^{13}	0	5 148	Emdee et al.[58]
R83	$c\text{-}C_6H_8 + OH = c\text{-}C_6H_6O + H + H_2$	5.00×10^{13}	0	0	Miller and Melius[43,j]
R84	$c\text{-}C_6H_7 + O_2 = c\text{-}C_6H_6O + OH$	2.60×10^{13}	0	2 000	Frank et al.[45,k]
R85	$c\text{-}C_6H_7 + O_2 = c\text{-}C_5H_7 + CO_2$	1.00×10^{13}	0	0	Alzueta et al.[46]
	Reactions of C_4H_6, C_4H_7, and C_4H_8				
R86	$CH_2CHCHCH_2 = CH_2CHCHCH + H$	7.00×10^{14}	0	94 990	Hidaka et al.[59]
R87	$CH_2CHCHCH_2 = CH_2CHCCH_2 + H$	7.00×10^{14}	0	94 990	Hidaka et al.[59]
R88	$CH_2CHCHCH_2 + H = CH_2CHCCH_2 + H_2$	3.90×10^{5}	2.5	5 820.0	Tsang[60,l]
R89	$CH_2CHCHCH_2 + OH = CH_2CHCCH_2 + H_2O$	1.11×10^{6}	2.0	1 450.0	Tsang[61,l]
R90	$NC_4H_7 = CH_2CHCHCH_2 + H$	1.00×10^{12}	0	38 000	this work for 30 Torr
R91	$BC_4H_7 = CH_2CHCHCH_2 + H$	3.16×10^{11}	0	34 800	this work for 30 Torr
R92	$NC_4H_7 = CH_3CHCCH_2 + H$	1.49×10^{11}	0.84	59 810	Tsang and Walker[62,m]
R93	$NC_4H_7 + H = CH_3CHCCH_2 + H_2$	1.81×10^{13}	0	0	Tsang[61,n]
R94	$NC_4H_7 + O_2 = CH_3CHCCH_2 + HO_2$	1.21×10^{12}	0	13 550	Tsang[61,n]
R95	$NC_4H_7 + OH = CH_3CHCCH_2 + H_2O$	6.02×10^{12}	0	0	Tsang[61,n]
R96	$NC_4H_7 + CH_3 = CH_3CHCCH_2 + CH_4$	3.01×10^{12}	−0.32	−130	Tsang[61,n]
R97	$BC_4H_7 = NC_4H_7$	2.37×10^{8}	0.88	29 600	Matheu et al.[35]
R98	$BC_4H_7 + H = C_4H_8\text{-}1$	2.00×10^{14}	0	0	Doute et al.[53]

[a] For a detailed description of generic rates, please refer to our earlier paper.[16] [b] Reference reaction $CH_3CH_2CH_2CH_2 = CH_3CH_2CHCH_2 + H$. [c] Reference reaction $CH_2CHCH_2CH_2 = CH_2CHCHCH_2 + H$. [d] The energy term was scaled according to the suggestion by Dean[37] for vinylic product. [e] Reference reaction $C_4H_7 = C_4H_6 + H$. [f] Reference reaction $CH_3CH(CH_3)CH_2 + X = CH_3C(CH_3)=CH_2 + HX$. [g] Reference reaction $c\text{-}C_6H_8 = bC_6H_6 + H_2$; A was adjusted higher by a factor of 10. [h] Reference reaction $(CH_3)_3CCHCH_2 = CH_3 + (CH_3)_2CCHCH_2$. [i] Reference reaction $C_2H_5CHCHCHCH_2 = CH_3 + CH_2CHCHCHCH_2$. [j] Reference reaction $C_6H_5 + OH = C_6H_5O + H$. [k] Reference reaction $C_6H_5 + O_2 = C_6H_5O + O$; E was adjusted lower by 4 kcal. [l] Reference reaction $C_3H_6 + X = CH_2CCH_3 + XH$. [m] Reference reaction $CH_2CHCH_2 = CH_2CCH_2 + H$. [n] Reference reaction $CH_2CHCH_2 + X = CH_2CCH_2 + XH$.

Thermal decomposition and hydrogen abstraction were identified to be the major consumption routes in flames of large paraffins.[30,31,32] Cyclohexane ($c\text{-}C_6H_{12}$), which consists of only secondary carbon atoms, should be no exception. In the extended mechanism, cyclohexane decomposes via hydrogen abstraction to cyclohexyl radical ($c\text{-}C_6H_{11}$) by the most powerful H (R1, 69%), OH (R2, 20%), and O (R3, 11%) radicals at

$$c\text{-}C_6H_{12} + H = c\text{-}C_6H_{11} + H_2 \quad (69\%) \quad \text{(R1)}$$

$$c\text{-}C_6H_{12} + OH = c\text{-}C_6H_{11} + H_2O \quad (20\%) \quad \text{(R2)}$$

$$c\text{-}C_6H_{12} + O = c\text{-}C_6H_{11} + OH \quad (11\%) \quad \text{(R3)}$$

generic rates, weighted by 12 to account for all possible sites, followed by minor hydrogen abstractors of CH_3 and HO_2 radicals and molecular O_2 (R4−R6), in order of their relative importance. The percent contribution presented in this work, unless otherwise stated, was calculated at 0.09 cm above the burner surface ($T = 1280$ K), where the measured benzene and enol concentrations reach their maximums. Reactions that involve enol species and numerical deviations will be discussed in part 2. The isomerization reaction R7 between cyclohexane and 1-hexene was proposed to be a possible fuel decomposition

$$c\text{-}C_6H_{12} = 1\text{-}C_6H_{12} \quad (<0.1\%) \quad \text{(R7)}$$

route.[33] The contribution of this reaction, however, is less than 1/1000 to the total fuel consumption rate under the conditions studied, likely due to the unstable biradical nature of the transition state.

A lumping technique was used to describe the decomposition of cyclohexyl radical ($c\text{-}C_6H_{11}$) in an earlier study.[34] The ring opening of the conjugate $c\text{-}C_6H_{11}$ radical was assumed to be the controlling step, the subsequent β scission of linear hexenyl radicals was assumed to be instantaneous, and the isomerization among linear hexenyl radicals was assumed to be critical in determining the product distribution. The resulting mechanism with lumped reaction pathways of $c\text{-}C_6H_{11}$ gave satisfactory results for the concentrations of a few selected species reported by Law.[8]

A rigorous approach was applied in the present work, and the extended mechanism includes separate elementary steps for consecutive ring opening, isomerization, and β scission for the decomposition of $c\text{-}C_6H_{11}$ radical. The majority of the $c\text{-}C_6H_{11}$ radical decomposes via β scission R8 (ring opening, 88%) at the generic rate and forms the linear 1-hexen-6-yl radical ($1\text{-}C_6H_{11}\text{-}6$), in addition to a minor pathway of unimolecular dehydrogenation (R17, 12%), which is the exclusive pathway

TABLE 2: Thermodynamic Data Estimated in the Utah Surrogate Mechanism, Which Are Compared with Those Reviewed in the NIST Chemistry WebBook[27,28] and by Burcat and Ruscic[29]

	Utah Surrogate Mechanism								literature values		
			C_p/R at temperature K								C_p/R,
species	$\Delta_f H°/RT$	$S°/R$	300	500	800	1000	1200	1500	$\Delta_f H°/RT$	$S°/R$	1000 K
									NIST Chemistry WebBook		
c-C_6H_{12}	−49.78	35.78	12.77	22.91	33.53	38.21	41.33	44.85	−49.68 ± 0.32	35.86	37.81
c-C_6H_{10}	−2.25	37.29	12.72	21.48	30.00	33.49	36.10	39.10	−1.74 ± 0.40	37.34	33.15
c-C_6H_8	44.07	38.10	14.91	21.31	27.98	30.91	32.80	34.99	42.21 ± 0.25[a]		29.40[a]
									42.28 ± 0.24[b]		29.31[b]
bC_6H_6	33.46	32.39	10.02	16.73	23.09	25.69	27.33	29.35	33.47 ± 0.20		25.43
fC_6H_6	85.42	34.13	17.39	19.60	22.33	23.80	25.76	30.96	90.41		
C_4H_6-13	47.77	35.45	9.35	13.80	18.84	20.78	22.01	23.55	45.16 ± 0.39		20.82
C_2H_4	21.17	26.36	5.15	7.52	10.09	11.33	12.19	13.20	21.18	26.38	11.29
C_2H_5	48.52	29.71	5.97	8.46	11.43	12.91	14.03	15.20	48.03 ± 0.81		
$C_6H_{11}CH_3$	−62.17	42.29	16.33	27.69	39.65	44.65	47.87	50.40	−62.48 ± 0.40	41.29	43.79
$C_6H_9CH_3$	−15.87	41.48	15.57	25.75	35.66	39.72	42.61	46.03	−32.79 ± 0.32[c]		
$C_6H_5CH_3$	20.26	39.34	12.66	20.30	28.02	31.39	33.82	36.30	20.18 ± 0.25		
c-C_6H_6O	−28.72	38.59	11.88	18.99	25.73	28.46	30.29	32.08	−28.25 ± 4.04		
1-C_6H_{12}	−16.85	46.52	15.88	23.92	32.27	36.06	38.87	41.80	−16.99		
NC_3H_7	40.61	34.81	8.89	13.03	17.41	19.44	20.98	22.60	40.36 ± 0.81		
									Burcat and Ruscic		
c-C_6H_{11}	30.18	38.28	12.61	22.20	32.11	36.48	39.29	42.65	30.61 ± 3.23	38.19	34.63
1-C_6H_{11}-6	64.21	47.13	15.86	23.33	30.82	34.21	36.52	39.47	65.58 ± 3.23	50.24	33.85
c-C_6H_9-3	32.99	38.65	12.44	20.59	28.47	31.66	34.00	36.84	53.05 ± 3.23	37.22	30.93
c-C_6H_9-4	77.74	38.68	12.56	20.77	28.59	31.76	34.07	36.89			
CC_6H_7	84.32	36.24	10.25	17.64	24.95	27.97	29.99	31.89	80.95 ± 14.13	36.78	27.97
CH_3-c-C_5H_4	91.38	38.59	11.77	18.82	25.18	27.71	29.50	31.39	91.52 ± 5.05	37.81	27.61
BC_4H_7	54.54	35.03	10.56	15.34	20.18	22.36	24.01	25.75	54.93 ± 3.23	36.81	21.75
PC_4H_9	26.71	38.44	11.68	17.19	22.97	25.64	27.65	29.80	33.01 ± 3.23	36.99	25.73
CH_3-c-C_5H_5	42.35	35.71	11.04	18.67	25.96	28.99	31.14	33.35	45.30 ± 3.23	37.38	28.62
1-C_6H_{11}-1	79.91	46.62	15.57	22.97	30.59	34.03	36.38	39.38			
1-C_6H_{11}-2	78.39	47.06	15.45	22.72	30.23	33.70	36.08	39.11			
1-C_6H_{11}-3	34.31	45.42	15.47	22.90	30.70	34.23	36.66	39.73			
$C_6H_7CH_3$	33.03	40.13	17.88	26.36	34.37	37.55	39.90	42.63			

[a] 1,3-Cyclohexadiene. [b] 1,4-Cyclohexadiene. [c] 1-Methylcyclohexene.

for the formation of cyclohexene (c-C_6H_{10}), in comparison with hydrogen abstraction reactions R18−R22.

$$\text{c-}C_6H_{11} = \text{1-}C_6H_{11}\text{-6} \quad (88\%) \qquad \text{(R8)}$$

$$\text{c-}C_6H_{11} = \text{c-}C_6H_{10} + H \quad (12\%) \qquad \text{(R17)}$$

Beta scission routes are dominant decomposition pathways of alkyl radicals in *n*-heptane and isooctane fuels[16] in comparison with competing isomerization reactions. In contrast, cyclohexane provides a very unique case in that its decomposition routes in flames are dominated by intramolecular hydrogen abstraction (or isomerization) between fuel conjugate and linear 1-hexenyl radicals. The isomerization between conjugate alkyl radicals was not considered in the study by Westmoreland and co-workers.[21]

The formation channel R12 of molecular ethylene and 1-buten-4-yl radical (BC_4H_7) via β scission at the generic rate,

$$\text{1-}C_6H_{11}\text{-6} = BC_4H_7 + C_2H_4 \quad (32\%) \qquad \text{(R12)}$$

for example, accounts for only 32% of the total fuel decomposition rate, although these two species are the natural products of 1-hexen-6-yl radical without hydrogen migration. The most important decomposition channel of linear hexenyl radicals is the formation of ethyl radical and molecular 1,3-butadiene (R13, 55%) at the generic rate, via an intermediate 1-hexen-3-yl radical (1-C_6H_{11}-3) that is formed via isomerization (R9), which was

$$\text{1-}C_6H_{11}\text{-6} = \text{1-}C_6H_{11}\text{-3} = C_2H_5 + C_4H_6 \quad (55\%) \qquad \text{(R9/R13)}$$

assigned the generic rate for a 1−4 and primary−secondary hydrogen migration with the energy barrier adjusted lower by 1 kcal/mol because the resonant structures of 1-C_6H_{11}-3 radical make the hydrogen migration more preferred.

In contrast, the 1−5 or 1−6 hydrogen migrations that lead to vinylic 1-hexen-2-yl (1-C_6H_{11}-2, R10) and 1-hexen-1-yl (1-C_6H_{11}-1, R11) radicals are less preferred. These two reactions were assigned the generic rates that correspond to their transient ring structure, with the energy barrier adjusted higher by 2 kcal/mol due to the stronger vinylic C−H bond. A 1−2 hydrogen migration of the 1-C_6H_{11}-3 radical might provide a plausible formation route of the 1-C_6H_{11}-4 radical. The product channel that involves the 1-C_6H_{11}-4 radical, therefore, was included to be a competing decomposition reaction (R14) of the 1-C_6H_{11}-3

$$\text{1-}C_6H_{11}\text{-3} = CH_3 + \text{L-}C_5H_8 \quad (0.3\%) \qquad \text{(R14)}$$

$$\text{1-}C_6H_{11}\text{-6} = \text{1-}C_6H_{11}\text{-2} = AC_3H_4 + NC_3H_7 \quad (0.4\%) \qquad \text{(R10/R16)}$$

$$\text{1-}C_6H_{11}\text{-6} = \text{1-}C_6H_{11}\text{-1} = C_2H_2 + PC_4H_9 \quad (0.2\%) \qquad \text{(R11/R15)}$$

radical, with the assumption that the hydrogen migration is the controlling step, the rate of which was estimated from a reference reaction of C_4H_7.[35] Formation reactions of products of the fuel consumption, such as C_2H_2, C_2H_4, C_2H_5, CH_2CCH_2, C_3H_7, 1,3-C_4H_6, C_4H_7 (1-buten-4-yl), and C_4H_9, will be discussed later.

In summary, the ring-opening step leads to a further branching of product distribution via subsequent isomerization among linear hexenyl radicals via an intramolecular transient ring that consists of five to seven atoms, and β scission pathways of these

radicals. The consumption rates of the 1-hexenyl isomers that include 1-C_6H_{11}-1, 1-C_6H_{11}-2, 1-C_6H_{11}-3, and 1-C_6H_{11}-6 radicals were found to be in equilibrium with the formation rates; the final branching ratios that are represented by percentages of the total fuel consumption rate for all product channels of ring opening (32 + 55 + 0.3 + 0.4 + 0.2%) and dehydrogenation (12%), therefore, add up to unity.

Benzene Formation via Cascading Dehydrogenation. Competing decomposition pathways of the conjugate cyclohexyl radical (c-C_6H_{11}) via cascading dehydrogenation have also been investigated. Cyclohexyl radical (c-C_6H_{11}) can be consumed via unimolecular dehydrogenation (R17) to form c-C_6H_{10}, the rate

$$\text{c-}C_6H_{11} = \text{c-}C_6H_{10} + H \quad (12\%) \qquad \text{(R17)}$$

of which was estimated to be $(1.0 \times 10^{14})e^{-38000/RT}$ (see Table 1 for units) after consulting with rates of similar reactions in the literature. These reference reactions include the dehydrogenation of a non-primary hexyl radical that forms an internal olefin, tetramethylethylene, at the rate of $(6.31 \times 10^{13})e^{-35570/RT}$ proposed by Baldwin et al.[36] (<130 Torr), and that of a primary butyl radical that leads to 1-butene at the rate of $(1.0 \times 10^{14})e^{-38350/RT}$ by Dean.[37] Reaction R17 accounts for 12% of the total c-C_6H_{11} radical decomposition, in comparison with 55% from the β scission R13, and 32% from reaction R12. The conjugate c-C_6H_{11} radical can also be consumed via hydrogen abstraction by O_2 (R18), which was assigned the generic rate. Reaction R18 is trivial at the location of the maximum benzene

$$\text{c-}C_6H_{11} + O_2 = \text{c-}C_6H_{10} + HO_2 \qquad \text{(R18)}$$

concentration, but it is the fastest c-C_6H_{10} formation route near the burner surface. Its rate at the burner surface is about 30 times higher than that of the unimolecular dehydrogenation (R17), 41% that of the β scission of the 1-C_6H_{11}-3 radical (R13), and about 20 times higher than that of the β scission of the 1-C_6H_{11}-6 radical (R12). The abstraction reactions with H, OH, O, and CH_3 radicals (R19−R22), the rates of which were proposed by Tsang,[38] make trivial contributions to the c-C_6H_{10} formation.

Hydrogen abstraction reactions with the most powerful H (35 + 34%), OH (10 + 10%), and O (6 + 6%) radicals were found to be the major consumption pathways of c-C_6H_{10}. Two cyclohexenyl isomers are formed from these abstraction reactions R24−R26 and R31−R33, denoted by c-C_6H_9-3 and c-C_6H_9-4 according to the radical site. Trivial hydrogen abstraction pathways R27−R29 and R34−R36 that involve molecular O_2 and CH_3 and HO_2 radicals were also included in the mechanism. All hydrogen abstraction reactions were assigned the generic rates for secondary carbons.

$$\text{c-}C_6H_{10} + H = \text{c-}C_6H_9\text{-}3 + H_2 \quad (35\%) \qquad \text{(R24)}$$

$$\text{c-}C_6H_{10} + OH = \text{c-}C_6H_9\text{-}3 + H_2O \quad (10\%) \qquad \text{(R25)}$$

$$\text{c-}C_6H_{10} + O = \text{c-}C_6H_9\text{-}3 + OH \quad (6\%) \qquad \text{(R26)}$$

$$\text{c-}C_6H_{10} + H = \text{c-}C_6H_9\text{-}4 + H_2 \quad (34\%) \qquad \text{(R31)}$$

$$\text{c-}C_6H_{10} + OH = \text{c-}C_6H_9\text{-}4 + H_2O \quad (10\%) \qquad \text{(R32)}$$

$$\text{c-}C_6H_{10} + O = \text{c-}C_6H_9\text{-}4 + OH \quad (6\%) \qquad \text{(R33)}$$

Cyclohexenyl radicals decompose mainly via the dehydrogenation reactions R40 (51%) and R44 (16%), and the β scission reaction R45 (33%), in comparison with hydrogen abstraction pathways that are at least 2 orders of magnitude slower. Weissman and Benson[39] proposed the rate for a similar formation reaction of 1,3-butadiene from 1-buten-4-yl radical ($CH_2{=}CHCH_2CH_2$) at atmospheric pressure. It is expected that the formation rates of 1,3-cyclohexadiene (c-C_6H_8) at 30 Torr in reactions R40 and R44 would be much smaller, and we found that a reduction by 1 order of magnitude in the prefactor in the reference rate would result in an excellent prediction for the concentration profile of c-C_6H_8. Cyclohexenyl radicals can also be consumed via hydrogen abstraction with molecular O_2 and H and OH radicals (R37−R39, R41−R43), using the same rates as for the cyclohexyl radical (c-C_6H_{11}) decomposition. The trivial abstraction reactions with O_2 (R37 and R41) at locations where benzene reaches its maximum concentration are, however, the major consumption pathways near the burner surface, and the rates of reactions R37 and R41 are 2 orders of magnitude higher than those of the unimolecular dehydrogenation reactions R40 and R44.

$$\text{c-}C_6H_9\text{-}3 + O_2 = \text{c-}C_6H_8 + HO_2 \qquad \text{(R37)}$$

$$\text{c-}C_6H_9\text{-}3 \rightleftharpoons \text{c-}C_6H_8 + H \quad (51\%) \qquad \text{(R40)}$$

$$\text{c-}C_6H_9\text{-}4 + O_2 = \text{c-}C_6H_8 + HO_2 \qquad \text{(R41)}$$

$$\text{c-}C_6H_9\text{-}4 = \text{c-}C_6H_8 + H \quad (16\%) \qquad \text{(R44)}$$

$$\text{c-}C_6H_9\text{-}4 = C_2H_3 + CH_2CHCHCH_2 \quad (33\%) \qquad \text{(R45)}$$

Also, possible c-C_6H_9 thermal decomposition reactions were considered, which represent combined elementary steps of the ring opening and the subsequent β scission of c-C_6H_9 isomers. In contrast to the decomposition of c-C_6H_{11} radical, composite reactions of c-C_6H_9 isomers in the extended mechanism do not involve isomerization after the ring opening since these reactions will generate highly unstable intermediates with vinylic moieties. Also, corresponding reactions that involve the more stable allylic c-C_6H_9-3 radical were not included as well, because a higher energy barrier of ring opening is associated with the formation of 1,3-hexadien-6-yl radical, in comparison with the barrier for the formation of allylic 1,5-hexadien-3-yl radical from the less stable c-C_6H_9-4 radical. Thermal decomposition of c-C_6H_9 radicals, therefore, includes fewer reactions. The formation of vinyl radical and molecular 1,3-butadiene via a β scission of the 1,5-hexadien-3-yl radical (R45) was assigned the generic rate of β scission, but was scaled with an increment in the energy term by 10 kcal/mol that was suggested by Dean[37] for the formation of vinylic radicals. In summary, the less preferred composite ring-opening pathway via the β scission R45 (33%) among all decomposition reactions of c-C_6H_9 radicals, in comparison with similar reactions that involve the c-C_6H_{11} radical (R12−R16, 88%), reflects the higher reaction barrier for the decomposition of 1,5-hexadien-3-yl radical, in addition to fewer β scission channels due to slow isomerization outlets. In contrast, the dehydrogenation pathways (R37−R44) are more preferable since they produce cyclohexadiene (c-C_6H_8), a more stable diene species due to the conjugate delocalized π-electron system, in comparison with a single double bond in c-C_6H_{10}.

The hydrogen abstraction reactions with H (R46, 60%), OH (R47, 17%), and O (R48, 5%) radicals were found to be the major decomposition pathways of cyclohexadiene (c-C_6H_8).

$$\text{c-}C_6H_8 + H = \text{c-}C_6H_7 + H_2 \quad (60\%) \qquad \text{(R46)}$$

$$\text{c-}C_6H_8 + OH = \text{c-}C_6H_7 + H_2O \quad (17\%) \qquad \text{(R47)}$$

$$\text{c-}C_6H_8 + O = \text{c-}C_6H_7 + OH \quad (5\%) \qquad \text{(R48)}$$

These reactions of c-C_6H_8 are very favorable due to the emerging aromaticity. The strength of C−H σ bond on an sp^3 carbon in c-C_6H_8 is 22.5 kcal/mol weaker than that on an sp^3 C−H bond in c-C_6H_{12}.[40] Dombi and co-workers[41] proposed the ratio of allylic hydrogen abstraction (2-butene + H, 6 hydrogen at both ends) over paraffinic hydrogen abstraction (propane + H, 6 hydrogen at both ends) at pressures from 50 to 100 Torr and temperatures between 779 and 812 K. At 800 K, the ratio is about 39, and an extrapolation to 1000 K yields a ratio of 17. Reactions R46−R48 of c-C_6H_8, therefore, were assigned rates 3 times the generic rates of hydrogen abstraction for secondary carbons, with a reduction in the energy term of 1.5 kcal/mol, in order to account for the greater stability due to the delocalization of five π electrons. At 1000 K, the adjustment yields a ratio of 19 for hydrogen abstraction rates (allylic vs paraffinic) per hydrogen. In addition, a formation route (R83)

$$\text{c-}C_6H_8 + OH = \text{c-}C_6H_6O + H + H_2 \quad (17\%) \quad \text{(R83)}$$

of cyclohexadienone (c-C_6H_6O, 17%) was included, and the reaction represents combined steps of the OH addition, the dehydrogenation, and the emission of molecular H_2. The rate of OH addition onto phenyl radical proposed by Miller and Melius[43] was taken for the composite reaction. The reaction was found to be critical in reproducing concentration profiles of cyclopentadiene and its radical.

Reaction classes that were identified to be critical to the decomposition of the analogous species cyclohexyl (c-C_6H_{11}) and cyclohexenyl (c-C_6H_9) radicals were found, again, to be the most important decomposition pathways for cyclohexadienyl radical (c-C_6H_7). No ring opening of the c-C_6H_7 radical, however, was considered since these reactions would require a rupture of a double bond. The dehydrogenation reaction R53 that forms benzene (bC_6H_6) accounts for 81% of the total consumption rate of the c-C_6H_7 radical, complemented by minor routes via isomerization (R57, 8%) and oxidation (R84, 6%; R85, 5%). Dean[37] and Mebel[42] suggested comparable rates for

$$\text{c-}C_6H_7 = \text{b}C_6H_6 + H \ (81\%) \quad \text{(R53)}$$

$$\text{c-}C_6H_7 = CH_3\text{-c-}C_5H_4 \ (8\%) \quad \text{(R57)}$$

$$\text{c-}C_6H_7 + O_2 = \text{c-}C_6H_6O + OH \ (6\%) \quad \text{(R84)}$$

$$\text{c-}C_6H_7 + O_2 = \text{c-}C_5H_7 + CO_2 \ (5\%) \quad \text{(R85)}$$

reaction R53 at the high-pressure limit, and a downward adjustment in the prefactor of the Dean rate by a factor of 40 led to good agreement between the predicted and measured concentration profiles of the c-C_6H_7 radical and benzene in the low-pressure flame studied. Hydrogen abstraction reactions of c-C_6H_7 radical (R54−R56), which were assigned the same rates used for c-C_6H_9 and c-C_6H_{11} radicals, made trivial contributions to the consumption of the c-C_6H_7 radical, with the exception of R54 (with O_2) being the fastest route at the burner surface.

The isomerization between c-C_6H_7 and CH_3-c-C_5H_4 radicals was assigned the rate that was proposed by Ritter et al.[44] The oxidation of c-C_6H_7 radical gives two major products: the formation of 2,4-cyclohexadienone (c-C_6H_6O, R84) via an elimination of an OH radical, the rate of which was estimated after a similar reaction of phenyl radical,[45] and the formation of cyclopentenyl radical (c-C_5H_7, R85) via an ejection of a CO_2, which was assigned the rate of a similar reaction of phenoxy radical proposed by Alzueta et al.[46]

Toluene Formation via Cascading Dehydrogenation. The cascading dehydrogenation mechanism of analogous methylcyclohexane ($C_6H_{11}CH_3$), methylcyclohexene ($C_6H_9CH_3$), methylcyclohexadiene ($C_6H_7CH_3$), and toluene ($C_6H_5CH_3$) was discussed in detail elsewhere.[16] Those reactions were assigned generic rates by assuming the hydrogen abstraction to be the controlling step and the subsequent dehydrogenation and dealkylation to be instantaneous. Consumption reactions of $C_6H_9CH_3$ and $C_6H_7CH_3$, for example, are summarized here, and readers should refer to our earlier paper for details.

$$C_6H_9CH_3 + H = C_6H_7CH_3 + H + H_2 \quad (31\%) \quad \text{(R72)}$$

$$C_6H_9CH_3 + OH = C_6H_7CH_3 + H + H_2O \quad (10\%) \quad \text{(R73)}$$

$$C_6H_9CH_3 + H = \text{c-}C_6H_8 + CH_3 + H_2 \quad (37\%) \quad \text{(R74)}$$

$$C_6H_9CH_3 + OH = \text{c-}C_6H_8 + CH_3 + H_2O \quad (10\%) \quad \text{(R75)}$$

$$C_6H_9CH_3 + H = \text{c-}C_6H_{10} + CH_3 \quad (11\%) \quad \text{(R76)}$$

$$C_6H_7CH_3 + H = C_6H_5CH_3 + H + H_2 \quad (47\%) \quad \text{(R77)}$$

$$C_6H_7CH_3 + OH = C_6H_5CH_3 + H + H_2O \quad (10\%) \quad \text{(R78)}$$

$$C_6H_7CH_3 + H = C_6H_6 + CH_3 + H_2 \quad (24\%) \quad \text{(R79)}$$

$$C_6H_7CH_3 + OH = C_6H_6 + CH_3 + H_2O \quad (4\%) \quad \text{(R80)}$$

$$C_6H_7CH_3 + H = \text{c-}C_6H_8 + CH_3 \quad (15\%) \quad \text{(R81)}$$

The new addition of cyclohexane and the existing methylcyclohexane subsets were bridged by the combination reactions R68−R71. It is noted that the reverse reaction R68 dominates in the cyclohexane flame studied, and accounts for 15% of the c-C_6H_{11} consumption at the burner surface. The rate used in the extended mechanism for reaction R68 was proposed by Brown and King[47] for low-pressure conditions. A few other reactions also help to interweave together the formation submechanisms of the first aromatic ring. The reactions of hydrogen abstraction followed by dealkylation R74, R75, R79, and R80, for example, lead to the formation of cyclohexa moieties with higher hydrogen deficiency from methylcyclohexa moieties, and those reactions of hydrogen addition followed by dealkylation R76, R81, and R82 produce species with the same degree of hydrogen deficiency.

In summary, the formation of the first aromatic ring in flames of cyclohexane and its derivatives exclusively depends on the cascading and interweaving dehydrogenation of the fuel, the kinetics of which were discussed elsewhere.[16]

Results and Discussion

The experimental temperature profile measured by Law[8] as shown in Figure 1 was used in the simulation, although Law suggested a shift of 0.05 cm downstream to account for possible probe effects. The temperature profile, however, was kept intact since the shift leads to slightly better predictions for the profiles of the major products only, but resulted in significant deviations of the predicted molecular oxygen profile in comparison with experimental data. Predicted and experimental concentrations of selected species that were measured in the cyclohexane flame[8,21] are compared in Figures 2−5.

Major Species. The predicted concentration profiles of molecular oxygen (O_2), argon, and major combustion products

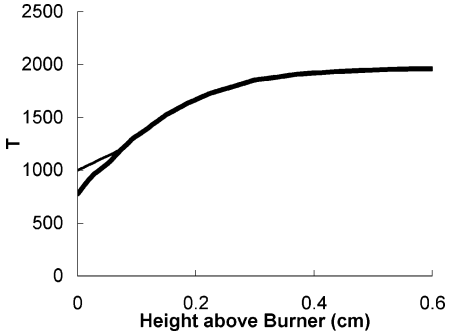

Figure 1. Experimental temperature profile that was used in the simulation (heavy solid line). The thin solid line is a temperature profile with the burner surface temperature adjusted upward to 1000 K that was used to demonstrate temperature effects on predicted concentrations.

of hydrogen (H_2), water vapor (H_2O), and carbon oxides (CO and CO_2) are compared with the experimental data in Figure 2. The uncertainty in experimental measurements for these major species, with the exception of argon, is 5%. The simulated results were able to match the overall O_2 profile very well, with the exception of a slight overprediction about 18% at the burner surface. Experimental uncertainties due to probe effects are the most likely source for numerical deviation upstream of the flame, since higher deviations, in terms of atomic balance and element flux, were found near the burner surface[8,21] that are not seen at any other locations. Good agreement was also obtained between the predicted and experimental concentration profiles for the inert argon and most major gaseous products, with the exception of slightly higher deviations near the burner surface. The numerical results for species H_2O, CO, and CO_2 were within 5−10% of measured concentrations. The predicted H_2 concentrations were about 35% higher than measured values in the post flame zone, probably due to the mass discrimination effects for lighter species.[8]

It is noted that O_2 mole fraction almost reaches a constant, about 5% of the reaction mixture, after the reaction zone. In stoichiometric flames, intact molecular O_2 is expected among reaction products, which always include incomplete combustion products, such as H_2 (3% in the cyclohexane flame studied) and CO (10%). In addition, the profiles of these two flammable gaseous products show a peak at about 0.15 cm above the burner surface for H_2, and another at 0.25 cm for CO, since H_2 and CO are burned as fuels downstream due to the abundance of oxidant. The predicted maximum concentration of H_2 is 15% higher, and that of CO is 11% lower, than the measured values.

Intermediate Fuel Decomposition Products. The predicted concentrations of major intermediates that are formed immediately from the fuel decomposition are compared with the experimental data in Figure 3. The formation of these species involves hydrogen abstraction of the fuel (c-C_6H_{12}), the ring opening of the resulting conjugate cyclohexyl radical (c-C_6H_{11}), and the subsequent β scission of linear hexenyl isomers (C_6H_{11}) that yields 1-buten-4-yl radical ($CH_2CHCH_2CH_2$), molecular 1,3-butadiene ($CH_2CHCHCH_2$), and ethylene (C_2H_4).

No definite conclusion was made for the identity for mass 83 at 8.79 eV, because no species was reported in the literature with comparable ionization energy. The species were speculated to be linear C_6H_{11} isomers,[8,21] since the 1-hexen-6-yl radical (1-C_6H_{11}-6) is a natural product of ring opening, and subsequent isomerization reactions among C_6H_{11} radicals are fast pathways for hydrocarbon decomposition. The sum of the predicted concentrations of four linear C_6H_{11} isomers (1-C_6H_{11}-1, 1-C_6H_{11}-2, 1-C_6H_{11}-3, and 1-C_6H_{11}-6), therefore, is compared with the measured values in Figure 3.

The predictions for c-C_6H_{12}, c-C_6H_{11}, and C_6H_{11}, however, are not in agreement with the experimental data. The predicted concentration of c-C_6H_{12} at the burner surface, for example, is a factor of 2 higher than the measured value. The fuel fraction in the feed was 6.75%, and both the simulated (a factor of 4 lower than what was in the feed) and measured (a factor of 8 lower) concentrations at the burner surface suggested that the fuel concentration be determined by the fast back diffusion of major species from downstream locations, rather than by reaction kinetics of the fuel decomposition. The transport parameters for major species that were used in the Utah Surrogate Mechanism are well-known.[48] Therefore, the deviations for the C_6 species in Figure 3 are likely due to the uncertainties in temperature measurements or other sampling effects.

The temperature effect on diffusion was checked. Modeling studies indicated that a burner surface temperature higher than 1000 K was necessary to enhance diffusion in order to bring the predicted c-C_6H_{12} concentration at the burner surface closer to the measured value. The temperature effect on predicted concentrations of major products and soot precursors, are, fortunately, comparable to experimental errors, as shown in Figures 3−5, where predicted concentrations using a burner surface temperature at 1000 K for selected species, such as acetylene, benzene, and butadiene, are also presented. Major concerns reported by Law[8] in the measurements include c-C_6H_{12} fragmentation at the photon energy used, and the uncertain chemical identities of the species that were thought to be C_6H_{11} isomers. The measured concentrations of O_2, therefore, were used as the standard to validate the predicted fuel consumption rate.

The predicted maximum concentration of C_4H_6 species (the sum of three isomers 1,3-butadiene ($CH_2CHCHCH_2$), 1,2-butadiene (CH_3CHCCH_2), and 1-butyne (CH_3CH_2CCH)) matches the measured value exactly with a slightly earlier peak position that is 0.015 cm upstream. The two isomers of butadiene could not be identified in the experiment because almost identical values of ionization energy were reported in the literature. The simulation results indicate a 95/5% distribution between butadiene isomers with 1,3-butadiene as the major product. The β scission reaction R13 of 1-C_6H_{11}-3 radical accounts for 73% of the total $CH_2CHCHCH_2$ formation rate, in addition to minor routes via the combination reaction R86 (9%) and the composite reaction R45 (7%).

$$1\text{-}C_6H_{11}\text{-}3 = C_2H_5 + CH_2CHCHCH_2 \quad (73\%) \quad (R13)$$

$$CH_2CHCHCH_2 = CH_2CHCHCH + H \quad (9\%) \quad (R86)$$

$$c\text{-}C_6H_9\text{-}4 = C_2H_3 + CH_2CHCHCH_2 \quad (7\%) \quad (R45)$$

The major consumption reactions of $CH_2CHCHCH_2$ include hydrogen abstraction reactions that form C_4H_5 isomers (79%) and the combination with H (R90, 12%) that leads to 1-buten-3-yl radical ($CH_2CHCHCH_3$). It is noted that the C_4H_7 isomers are formed in the simulation via hydrogen addition onto 1,3-butadiene, as a consequence of isomerization among linear hexenyl radicals that were included in the extended mechanism. Law[8,21] reported the formation of 1,3-butadiene via the dehydrogenation of C_4H_7 species because isomerization was not included in their reaction mechanism. Other C_4H_6 isomers, such as 1- and 2-butyne, were not detected in the experiment, which is reflected by the simulated concentrations of 1-butyne that are about 3 orders of magnitude lower than those of 1,3-butadiene.

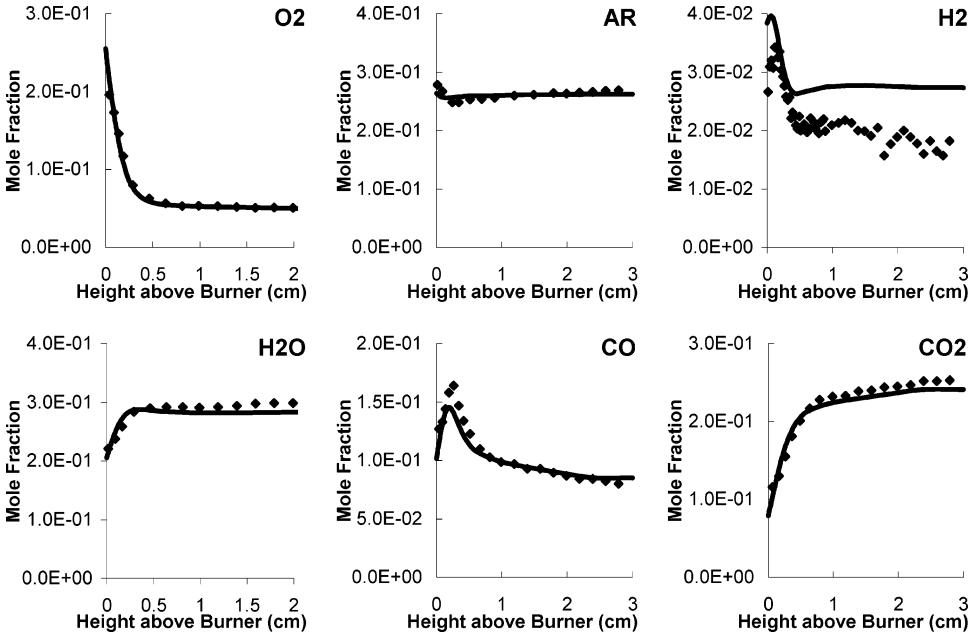

Figure 2. Comparisons between predicted and experimental concentration profiles of major species. The symbols represent the experimental data; the lines represent the simulations.

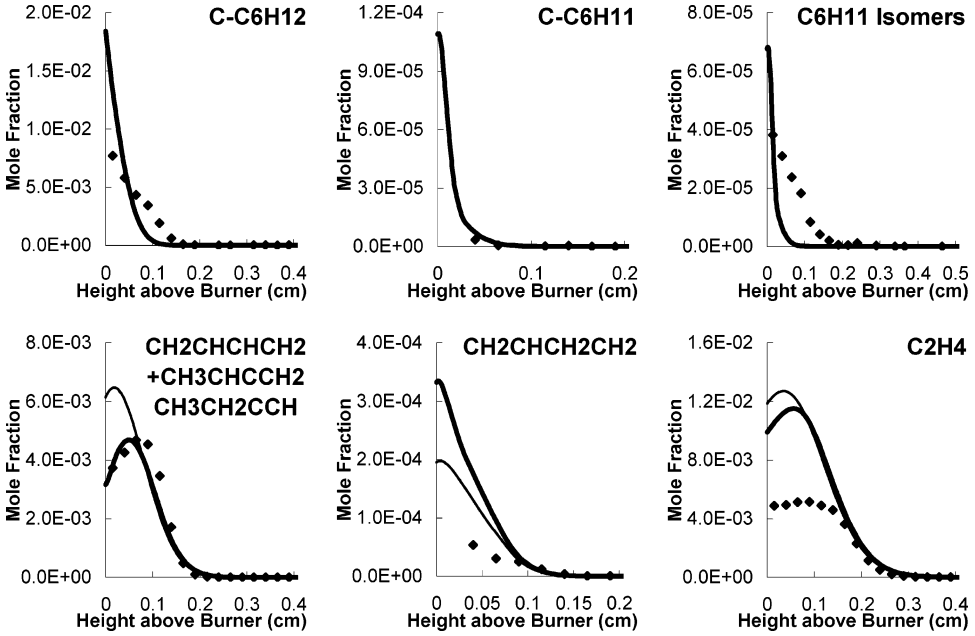

Figure 3. Comparisons between predicted and experimental concentration profiles of selected species from fuel decomposition. The symbols represent the experimental data; the heavy solid lines represent the simulations using experimental temperatures; the thin solid lines represent the simulations using experimental temperatures but with the burner surface temperature at 1000 K.

The C_4H_7 species detected in the experiment was believed to be 1-buten-4-yl radical ($CH_2CHCH_2CH_2$, BC_4H_7 in Table 1), although methyl allyl radical (IC_4H_7 in the Utah Surrogate Mechanism) has a closer reported ionization energy. Methyl allyl radical is not, however, the major C_4H_7 isomer since its likely parent species, such as methylcyclopentenyl radical (C_6H_9) and isobutylene, have too low mole fractions (10^{-6} in the simulation) in comparison with those of C_4H_7 (10^{-5}), in addition to no experimental evidence of existence. The predicted peak concentration of $CH_2CHCH_2CH_2$ radical at the burner surface was 7 times the measured value, likely due to uncertainties in the rate of the pressure-dependent combination reaction R91, which accounted for 99% of the $CH_2CHCH_2CH_2$ formation at the burner surface. The major $CH_2CHCH_2CH_2$ consumption routes include the combination reaction R98, which forms 1-butene (75%, at the burner surface), and hydrogen abstraction reactions (23%).

The predicted maximum concentration of ethylene was twice the experimental value. Uncertainties in reactions of ethyl radical are suspected to be responsible for the numerical deviation since the dehydrogenation (49%) and hydrogen abstraction (6%) of ethyl radical were identified to be the major formation routes of ethylene, in addition to other pathways via the β scission of 1-hexen-6-yl (R12, 17%) and 1-buten-3-yl (5%) radicals, and the hydrogen addition to 1-butene (7%) and propylene (8%) followed by β scission. Modifications that involve competing consumption reactions of ethyl radical, therefore, may lead to lower prediction of ethylene. Consumption reactions of ethylene include oxidation ($C_2H_4 + O =$ products, 46%) and hydrogen abstraction ($C_2H_4 + X = C_2H_3 + HX$, 45%) of equal

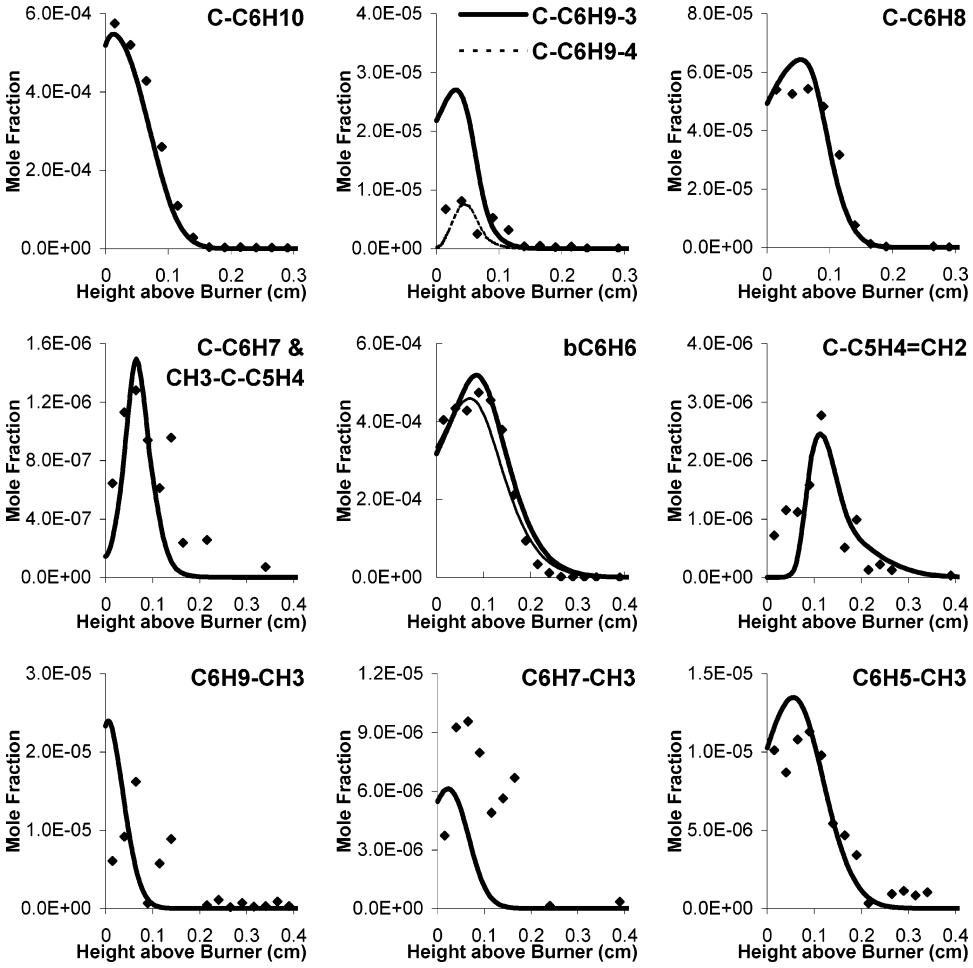

Figure 4. Comparisons between predicted and experimental concentrations in cascading dehydrogenation. The symbols represent the experimental data; the heavy solid lines represent the simulations using experimental temperatures; the thin solid lines represent the simulations using experimental temperatures but with the burner surface temperature at 1000 K.

importance. Another noteworthy ethylene consumption reaction is the OH radical addition (5%) that leads to the formation of ethenol (CH_2CHOH), a tautomer of more stable acetaldehyde (CH_3CHO). The significance in formation of enol species, such as CH_2CHOH, resides in the partial oxidation in combustion that always leads to emission of pollutants. Reactions of enol species will be discussed in detail in part 2.

Cascading Dehydrogenation. The measured concentrations of cyclohexene (c-C_6H_{10}), cyclohexadiene (c-C_6H_8), and their radicals, which are immediate products of the fuel consumption via the cascading dehydrogenation, were very well reproduced, as shown in Figure 4. The predicted maximum concentration of c-C_6H_{10}, for example, is only 4.7% lower than the measured value, with a slightly upstream profile by 0.01 cm. The product branching ratio between the benzene formation and the ring opening was estimated to be 12/88% in the simulation for the decomposition of c-C_6H_{11} radical.

The cyclohexenyl (c-C_6H_9) isomers could not be distinguished in the experiment because the same value of ionization energy was reported for the two most plausible isomers (c-C_6H_9-3 and c-C_6H_9-4). The predicted maximum concentration of c-C_6H_9 species (sum of these two isomers) is about 4 times that measured in the experiment. It is interesting to note that the predicted peak concentration of c-C_6H_9-4 radical is only about 7% lower than the experimental value. Possible unimolecular decomposition reactions of the more stable c-C_6H_9-3 isomer, which were not considered in the extended mechanism due to the higher energy for the transition state, are likely responsible for the overprediction. It is noted that the composite unimolecular decomposition reaction R45 accounts for two-thirds of the consumption of the c-C_6H_9-4 isomer. The product branching ratio between the cascading dehydrogenation and the ring opening was estimated to be 67/33% for the decomposition of c-C_6H_9 species.

The concentrations of c-C_6H_8 were well reproduced within 20% of the experimental data, although the plateau shape of the measured profile made it more difficult for the simulation to capture the trend upstream. The product branching ratio for c-C_6H_8 decomposition was estimated to be 82/17% between the cascading dehydrogenation and the oxidation reaction R83.

Good agreement was obtained between the measured and predicted concentrations of C_6H_7 species, which include three isomers in the extended mechanism. Unfortunately, the identity of C_6H_7 species could not be confirmed in the experiment because there were no reliable data of ionization energy reported for C_6H_7 isomers. Although only one species of mass 79 was detected in the experiment, the modeling results suggested an equal importance for the two major C_6H_7 isomers, with an estimated distribution of 40−45/50−55% between cyclohexadienyl (c-C_6H_7) and methylcyclopentadienyl (CH_3-c-$^{\bullet}C_5H_4$) radicals, both allylic, in addition to a trivial third isomer, vinylic methylcyclopentadienyl radical (CH_3-c-$C_5H_4^{\bullet}$, not included in Table 1). The predicted maximum concentration of C_6H_7 species (sum of three isomers) is only 16% higher than the measured value, and the position of the peak and the trend of the profile are also faithfully reproduced.

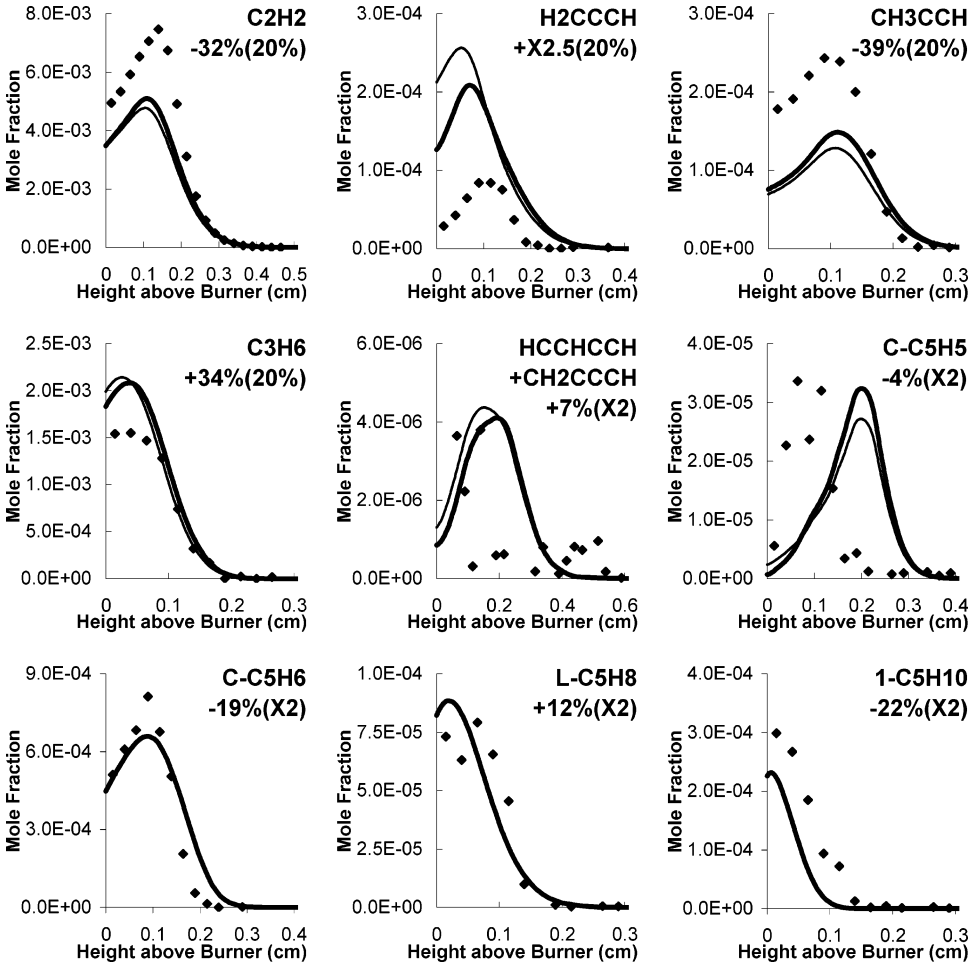

Figure 5. Comparisons between predicted and experimental concentration profiles of soot precursors. The symbols represent the experimental data; the heavy solid lines represent the simulations using experimental temperatures; the thin solid lines represent the simulations using experimental temperatures but with the burner surface temperature at 1000 K. *A*(*B*) indicates the numerical deviation of *A*% in comparison with the experimental uncertainty of *B*% for each species.

The major reaction routes of c-C_6H_7 radical involve mainly the formation of benzene as discussed earlier. The allylic methylcyclopentadienyl radical is formed exclusively via isomerization of c-C_6H_7 radical (R57). It is noted that the major consumption route of the CH_3-c-C_5H_4 radical via dehydrogenation and reorganization (R58) also leads to the formation of benzene (36%). Other significant consumption routes of the CH_3-c-C_5H_4 radical include the formation reaction R59 of fulvene (fC_6H_6) via dehydrogenation (29%), the formation reaction R63 of methylcyclopentadiene (CH_3-c-C_5H_5) via hydrogenation (15%), and the hydrogen addition reaction R64 (15%) followed by dealkylation.

$$bC_6H_6 + H = CH_3\text{-c-}C_5H_4 \quad (36\%) \quad (R58)$$

$$CH_3\text{-c-}C_5H_4 = fC_6H_6 + H \quad (29\%) \quad (R59)$$

$$CH_3\text{-c-}C_5H_4 + H = CH_3\text{-c-}C_5H_5 \quad (15\%) \quad (R63)$$

$$CH_3\text{-c-}C_5H_4 + H = CH_3 + C_5H_5 \quad (15\%) \quad (R64)$$

Both C_6H_7 isomers were found to be critical to the formation of the cyclic C_6H_6 isomers, namely benzene (bC_6H_6) and fulvene (fC_6H_6). Fulvene is formed mainly from the dehydrogenation reaction R59 of the allylic methylcyclopentadienyl radical CH_3-c-$^{\bullet}C_5H_4$ (72%), in addition to the minor formation routes via the dehydrogenation reaction R65 of methylcyclopentadiene CH_3-c-C_5H_5 (18%) and the hydrogen abstraction reactions R60−62 (11%). Hydrogen radical catalyzed isomerization to benzene (R66) was identified to be the major consumption route of fulvene (81%). Although the formation of fulvene via the combination of propargyl and allyl radicals (R67), and the subsequent isomerization (R66) was considered to be a major benzene formation route,[49] the reaction was found to progress in the direction of the reverse reaction that accounts for 18% of the fulvene consumption. Reaction R66 was found to be the major formation pathway of fulvene in another study[21] by Westmoreland and co-workers when cyclic species of fulvenic derivatives were not included in their mechanism. They reported an underprediction of a factor of 3 for fulvene, which might be considered as indirect evidence of the role of allylic methylcyclopentadienyl radical in the fulvene formation.

$$CH_3\text{-c-}C_5H_4 = fC_6H_6 + H \quad (72\%) \quad (R59)$$

$$CH_3\text{-c-}C_5H_5 = fC_6H_6 + H_2 \quad (18\%) \quad (R65)$$

$$fC_6H_6 + H = bC_6H_6 + H \quad (81\%) \quad (R66)$$

$$H_2CCCH + AC_3H_5 = fC_6H_6 + H + H \quad (18\%) \quad (R67)$$

Cascading dehydrogenation has been proposed in this work to be the major benzene formation mechanism, and the dehydrogenation reaction R53 of c-C_6H_7 radical was found to

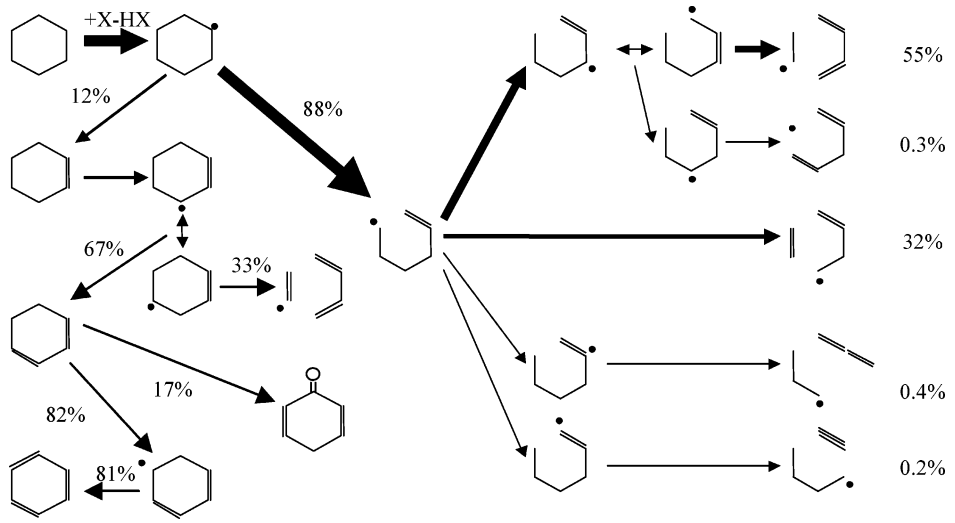

Figure 6. Major reaction pathways of cyclohexane. The major β scission pathways account for 88% (55 + 0.3 + 32 + 0.4 + 0.2%) of the total fuel consumption at 0.09 cm above the burner surface. Other percentages represent the branching ratios of corresponding precursor species.

account for 93% of the total benzene formation rate. Benzene, one of the most important soot precursors, was produced in cyclohexane flames from the fuel directly without further decomposition that forms smaller aromatic precursors, as seen in flames of most other fuels. The maximum benzene concentration was reported to be 473 ppm in the stoichiometric cyclohexane flame studied, in comparison with 12 ppm in a stoichiometric *n*-heptane flame.[16] The combination of propargyl radicals, a competing benzene formation route, is at least 3 orders of magnitude slower than the dehydrogenation reaction under the current flame conditions.

The formation of phenyl radical (C_6H_5) accounts for 65% of the benzene consumption. Competing benzene consumption routes include the oxidation reaction ($C_6H_6 + O$) that forms the phenoxy radical (C_6H_5O), which is a precursor for cyclopentadienyl radical.

The predicted benzene and fulvene concentrations are in very good agreement with the experimental data. The maximum concentration of benzene was overpredicted, for example, by 9.5% only, in comparison with the estimated uncertainty at 20% reported by Law.[8,21] The measured peak concentration of fulvene ($c\text{-}C_5H_4{=}CH_2$ in Figure 4) was underpredicted by 12%, and the experimental uncertainty for fulvene is 50%. The simulation results capture the trends of the concentration profiles for both C_6H_6 isomers nicely with very accurate predictions for the peak locations.

It is noted that the fulvene profile reaches its maximum at 0.115 cm above the burner surface, about 0.01−0.015 cm downstream of the benzene peak. While measured profiles of analogous series of $c\text{-}C_6H_{12}$, $c\text{-}C_6H_{10}$, $c\text{-}C_6H_8$, and bC_6H_6 suggest the importance of the cascading dehydrogenation, the relative peak positions of fulvene and benzene provides other conclusive evidence of the cascading dehydrogenation pathway in cyclohexane flames, since it infers the precursor characteristics of parent species of benzene with regard to those of fulvene, although about 2% of benzene formation was found to be from fulvene (R66). The parent species of fulvene, the allylic methylcyclopentadienyl radical ($CH_3\text{-}c^{\bullet}\text{-}C_5H_4$), is formed exclusively via isomerization from the parent species of benzene, the cyclohexadienyl radical ($c\text{-}C_6H_7$). In contrast, in flames with other fuels, e.g., in a stoichiometric *n*-heptane flame,[16] fulvene has an earlier peak than benzene since fulvene is a benzene precursor via reaction R66, and both isomers were formed from combination reactions of C_2-C_4 fragments. In summary, combination reactions are not important to the formation of C_6H_6 isomers in cyclohexane flames because, otherwise, we would expect an earlier peak location for the fulvene isomer.

Reactions of higher analogous species that are parallel to the reaction order between $c\text{-}C_6H_7$ and $CH_3\text{-}c\text{-}C_5H_4$ radicals, e.g., $c\text{-}C_6H_9$ and $CH_3\text{-}c\text{-}C_5H_6$, $c\text{-}C_6H_{11}$ and $CH_3\text{-}c\text{-}C_5H_8$, are also plausible pathways for fulvene formation via cascading dehydrogenation of the $CH_3\text{-}C_5$ ring. These reactions, however, were not considered in the current mechanism due to very few kinetic data available in the literature.

The measured profiles of methylcyclohexene ($C_6H_9\text{-}CH_3$), methylcyclohexadiene ($C_6H_7\text{-}CH_3$), and toluene ($C_6H_5\text{-}CH_3$), derivatives of the cyclohexene, cyclohexadiene, and benzene series, were also well predicted as shown in the third row of Figure 4. Cascading dehydrogenation was found to be the most important formation pathway for these analogous species, as discussed earlier. Unfortunately, methylcyclohexane ($C_6H_{11}\text{-}CH_3$), the source of this series, was not detected in the experiment. Otherwise, the combination reactions R69−R71, which interweave together the toluene and benzene submechanisms, can be more carefully examined. Scattered experimental data points made it more difficult for the model to reproduce the measured profiles of $C_6H_7\text{-}CH_3$ and its parent species $C_6H_9\text{-}CH_3$. The measured concentrations of $C_6H_9\text{-}CH_3$, for example, can be divided into three groups that probably have no statistical correlations among them. The numerical deviations for the predicted maximum concentrations of $C_6H_9\text{-}CH_3$, $C_6H_7\text{-}CH_3$, and $C_6H_5\text{-}CH_3$ were +34%, −36%, and +19%, respectively. It is noted that the predicted profiles of these species, with the exception of toluene, are slightly upstream.

Major fuel decomposition pathways in the cyclohexane flame and branching ratios of product channels for various intermediates are summarized in Figure 6.

Important Soot Precursors. Only a brief discussion on predictions of soot precursors is presented, and a more detailed description will be provided in part 2. Comparisons are presented with the experimental data in Figure 5 of the predicted concentrations of major soot precursors. Also, the numerical deviation and the estimated experimental uncertainty of each species are included. The major soot precursors that were studied include (1) acetylene and C_4H_3 species that are important in the HACA mechanism proposed by Frenklach et al.,[50] (2) propargyl radical and propyne, combination reactions of which were proposed to be the major benzene formation pathways,[43]

and (3) cyclopentadiene and its radical, a naphthalene precursor via self-combination.[51,52] Other important benzene precursors include (4) toluene in Figure 4, the dealkylation of which provides a minor benzene formation route, and (5) cyclohexene and cyclohexadiene in Figure 3, the dehydrogenation of which were identified to be the exclusive benzene formation route in the cyclohexane flame studied. The predicted concentrations of selected olefin and diene species are also compared with experimental data in Figure 5 because these species are closely related to the kinetics of soot precursor species. It is noted that the predicted profile of cyclopentadienyl radical is significantly downstream in comparison with the experimental data. In contrast, the prediction for molecular cyclopentadiene is quite satisfactory.

Conclusion

The Utah Surrogate Mechanism was extended to include a detailed description of the cyclohexane decomposition. Generic rates were assigned to relevant reaction classes. The approach was found to be adequate to reproduce experimental concentration profiles of major species and important intermediates, such as major soot precursors.

Ring-opening pathways via β scission compete with dehydrogenation routes for the conjugate cyclohexyl radical. The ring-opening channels include the formation of butadiene that involves a 1−4 internal hydrogen migration and the formation of $CH_2CHCH_2CH_2$, without any intramolecular isomerization. Besides decomposition reactions that form smaller fragments, cascading dehydrogenation also makes an important contribution to the fuel decomposition and provides the exclusive benzene formation pathway. Interweaving reactions between analogous species series, such as methylcyclohexane and cyclohexane, also influence the benzene formation. In contrast, combination reactions of smaller C_2-C_4 species were found to be insignificant toward benzene formation under current conditions studied.

Acknowledgment. This research was funded by the University of Utah (C-SAFE), through a contract with the Department of Energy, Lawrence Livermore National Laboratory (B341493).

Note Added after ASAP Publication. This article was released ASAP on February 23, 2007. Reactions 44 and 45 have been revised. The corrected version was posted on March 2, 2007.

References and Notes

(1) Hakansson, A.; Stromberg, K.; Pedersen, J.; Olsson, J. O. *Chemosphere* **2001**, *44* (5), 1243.

(2) Doute, C.; Delfau, J.-L.; Akrich, R.; Vovelle, C. *Combust. Sci. Technol.* **1995**, *106* (4−6), 327.

(3) Violi, A.; Yan, S.; Eddings, E. G.; Sarofim, A. F.; Granata, S.; Faravelli, T.; Ranzi, E. *Combust. Sci. Technol.* **2002**, *174*, 399.

(4) Zhang, H. R.; Eddings, E. G.; Sarofim, A. F. *Proc. Combust. Inst.* **2007**, *31*, 401.

(5) Cathonnet, M.; Voisin, D.; Etsonli, A.; Sferdean, C.; Reuillon, M.; Boettner, J. C.; Dagaut, P. Papers presented at the Applied Vehicle Technology Panel (AVT) Symposium, 1999, Lisbon, Oct 12−16, 1998; 14/1−14/9.

(6) Mawid, M. A.; Park, T. W.; Sekar, B.; Arana, C. *CPIA Publication (2002), 713 (26th JANNAF Airbreathing Propulsion Subcommittee Meeting)*; CPIA: Columbia, MD, 2002; Vol. 1, p 21.

(7) Cooke, J. A.; Bellucci, M.; Smooke, M. D.; Gomez, A.; Violi, A.; Faravelli, T.; Ranzi, E. *Proc. Combust. Inst.* **2005**, *30*, 439.

(8) Law, M. E. Ph.D. Dissertation, Department of Chemical Engineering, University of Massachusetts, Amherst, 2005.

(9) Siegel, W. O.; McCabe, R. W.; Chun, W.; Kaiser, E. W.; Perry, J.; Henig, Y. I.; Trinker, F. H.; Anderson, R. W. *J. Air Waste Manage. Assoc.* **1992**, *42* (7), 912.

(10) Voisin, D.; Marchal, A.; Reuillon, M.; Boettner, J.-C.; Cathonnet, M. *Combust. Sci. Technol.* **1998**, *138* (1−6), 137.

(11) Davis, S. G.; Law, C. K. *Combust. Sci. Technol.* **1998**, *140* (1−6), 427.

(12) Ristori, A.; Dagaut, P.; El Bakali, A.; Cathonnet, M. *Combust. Sci. Technol.* **2001**, *165*, 197.

(13) Braun-Unkhoff, M.; Naumann, C.; Frank, P. *Abstracts of Papers*, 227th National Meeting of the American Chemical Society, Anaheim, CA, March 28−April 1, 2004; American Chemical Society: Washington, DC, 2004; FUEL-173.

(14) Bennett, P. J.; Gregory, D.; Jackson, R. A. *Combust. Sci. Technol.* **1996**, *115* (1−3), 83.

(15) Ranzi, E.; Dente, M.; Goldaniga, A.; Bozzano, G.; Faravelli, T. *Prog. Energy Combust. Sci.* **2001**, *27* (1), 99.

(16) Zhang, H. R.; Eddings, E. G.; Sarofim, A. F. *Combust. Sci. Technol.* **2007**, *179*, 61.

(17) Klai, S. E.; Baronnet, F. *J. Chim. Phys. Phys.-Chim. Biol.* **1993**, *90* (10), 1951.

(18) El Bakali, A.; Braun-Unkhoff, M.; Dagaut, P.; Frank, P.; Cathonnet, M. *Proc. Combust. Inst.* **2000**, *38*, 1631.

(19) Granata, S.; Faravelli, T.; Ranzi, E. *Combust. Flame* **2003**, *132* (3), 533.

(20) Gon, S.; Law, M. E.; Westmoreland, P. R.; Cool, T. A.; Wang, J.; Hansen, N.; Taatjes, C. A.; Kasper, T.; Obwald, P. *Chem. Phys. Processes Combust.* **2005**, 221−224.

(21) Law, M. E.; Westmoreland, P. R.; Cool, T. A.; Wang, J.; Hansen, N.; Kasper, T. *Proc. Combust. Inst.* **2007**, *31*, 565.

(22) Kee, R. J.; Rupley, F. M.; Miller, J. A.; Coltrin, M. E.; Grcar, J. F.; Meeks, E.; Moffat, H. K.; Lutz, A. E.; Dixon-Lewis, G.; Smooke, M. D.; Warnatz, J.; Evans, G. H.; Larson, R. E.; Mitchell, R. S.; Petzold, L. R.; Reynolds, W. C.; Caracotsios, M.; Stewart, W. E.; Glarborg, P.; Wang, C.; Adigun, O.; Houf, W. G.; Chou, C. P.; Miller, S. F.; Ho, P.; Yang, D. J. *Chemkin Collection*, release 4.0; Reaction Design, Inc.: San Diego, CA, 2004.

(23) Kee, R. J.; Rupley, F. M.; Miller, J. A. *Sandia Natl. Lab. [Tech. Rep.] SAND* **1993**, *SAND-87-8215B.*

(24) Muller, C.; Michel, V.; Scacchi, G.; Côme, G. M. *J. Chim. Phys.* **1995**, *92*, 1154.

(25) Benson, S. W.; Cruickshank, F. R.; Golden, D. M.; Haugen, G. R.; O'Neal, H. E.; Rodgers, A. S.; Shaw, R.; Walsh, R. *Chem. Rev.* **1969**, *69*, 279.

(26) Kee, R. J.; Dixon-Lewis, G.; Warnatz, J.; Coltrin, M. E.; Miller, J. A. *Sandia Natl. Lab. [Tech. Rep.] SAND* **1986**, *SAND-86-8246*.

(27) Afeefy, H. Y.; Liebman, J. F.; Stein, S. E. Neutral Thermochemical Data. In *NIST Chemistry WebBook, NIST Standard Reference Database Number 69*; Linstrom, P. J., Mallard, W. G., Eds.; National Institute of Standards and Technology: Gaithersburg MD, 20899; June 2005 (http://webbook.nist.gov).

(28) Glushko Thermocenter, Russian Academy of Sciences, Moscow. Entropy and Heat Capacity of Organic Compounds. In *NIST Chemistry WebBook, NIST Standard Reference Database Number 69*; Linstrom, P. J., Mallard, W. G., Eds.; National Institute of Standards and Technology: Gaithersburg MD, 20899; June 2005 (http://webbook.nist.gov).

(29) Burcat, A.; Ruscic, B. *Third Millennium Ideal Gas and Condensed Phase Thermochemical Database for Combustion with updates from Active Thermochemical Tables*; ANL-05/20 and TAE 960 Technion-IIT, Aerospace Engineering, and Argonne National Laboratory, Chemistry Division, September 2005.

(30) Zhang, H. Ph.D. Dissertation, Department of Chemical Engineering, University of Utah, 2005.

(31) El Bakali, A.; Delfau, J. L.; Vovelle, C. *Combust. Flame* **1999**, *118*, 381.

(32) Curran, H. J.; Gaffuri, P.; Pitz, W. J.; Westbrook, C. K. *Combust. Flame* **1998**, *114*, 149.

(33) Tsang, W. *Int. J. Chem. Kinet.* **1978**, *10*, 1119.

(34) Zhang, H. R.; Huynh, L. M.; Kungwan, N.; Zhang, S.; Yang, Z.; Truong, T. N.; Eddings, E. G.; Sarofim, A. F. *Prepr. Pap.—Am. Chem. Soc., Div. Fuel Chem.* **2006**, *51* (1), 229.

(35) Matheu, D. M.; Green, W. H.; Grenda, J. M. *Int. J. Chem. Kinet.* **2003**, *35*, 95.

(36) Baldwin, R. R.; Drewery, G. R.; Walker, R. W. *J. Chem. Soc., Faraday Trans. 1* **1984**, *80*, 3195.

(37) Dean, A. M. *J. Phys. Chem.* **1985**, *89*, 4600.

(38) Tsang, W. *J. Phys. Chem. Ref. Data* **1990**, *19*, 1.

(39) Weissman, M.; Benson, S. W. *Int. J. Chem. Kinet.* **1984**, *16*, 307.

(40) Kerr, J. A.; Stocker, D. W. Strength of chemical bonds. *CRC Handbook of Chemistry and Physics*, 81st ed.; Lide, D. R., Ed. in Chief; CRC Press: Boca Raton, FL, 2000−2001; pp 9−64.

(41) Dombi, A.; Bozo, E.; Huhn, P. *Magy. Kem. Foly.* **1985**, *91*, 177.

(42) Mebel, A. M.; Lin, M. C.; Yu, T.; Morokuma, K. *J. Phys. Chem. A* **1997**, *101*, 3189.

(43) Miller, J. A.; Melius, C. F. *Combust. Flame* **1992**, *91*, 21.

(44) Ritter, E. R.; Bozzelli, J. W.; Dean, A. M. *J. Phys Chem.* **1990**, *94*, 2493.
(45) Frank, P.; Herzler, J.; Just, Th.; Wahl, C. *Proc. Combust. Inst.* **1994**, *25*, 833.
(46) Alzueta, M. U.; Glarborg, P.; Dam-Johansen, K. *Int. J. Chem. Kinet.* **2000**, *32*, 498.
(47) Brown, T. C.; King, K. D. *Int. J. Chem. Kinet.* **1989**, *21*, 251.
(48) Hirschfelder, J. O.; Bird, R. B.; Spotz, E. L. *Chem. Rev.* **1949**, *44*, 205.
(49) Marinov, N. M.; Pitz, W. J.; Westbrook, C. K.; Vincitore, A. M.; Castaldi, M. J.; Senkan, S. M. *Combust. Flame* **1998**, *114*, 192.
(50) Frenklach, M.; Clary, D. W.; Gardiner, W. C., Jr.; Stein, S. E. *Proc. Combust. Inst.* **1985**, *20*, 887.
(51) Cypres, R.; Bettens, B. *Tetrahedron* **1974**, *30*, 1253.
(52) Cypres, R.; Bettens, B. *Tetrahedron* **1975**, *31*, 359.
(53) Doute, C.; Delfau, J. L.; Vovelle, C. *Combust. Sci. Technol.* **1999**, *147*, 61.
(54) Alfassi, Z. B.; Benson, S. W.; Golden, D. M. *J. Am. Chem. Soc.* **1973**, *95*, 4784.
(55) Burcat, A.; Dvinyaninov, M. *Int. J. Chem. Kinet.* **1997**, *29*, 505.
(56) Trenwith, A. B. *Trans. Faraday Soc.* **1970**, *66*, 2805.
(57) Trenwith, A. B. *J. Chem. Soc., Faraday Trans. 1* **1980**, *76*, 266.
(58) Emdee, J.; Brezinsky, K.; Glassman, I. *J. Phys. Chem.* **1992**, *96*, 2151.
(59) Hidaka, Y.; Higashihara, T.; Ninomiya, N.; Oshita, H.; Kawano, H. *J. Phys. Chem.* **1993**, *97*, 10977.
(60) Tsang, W. *Ind. Eng. Chem. Res.* **1992**, *31*, 3.
(61) Tsang, W. *J. Phys. Chem. Ref. Data* **1991**, *20*, 221.
(62) Tsang, W.; Walker, J. A. *J. Phys. Chem.* **1992**, *96*, 8378.